Interaction of Carotenoids and Cu^{2+} in Cu-MCM-41: Distance-Dependent Reversible Electron Transfer

Yunlong Gao,[†] Tatyana A. Konovalova,[†] Jesse N. Lawrence,[†] M. A. Smitha,[†] Jolanta Nunley,[‡] Rainer Schad,[§] and Lowell D. Kispert*,[†]

Department of Chemistry, Box 870336, University of Alabama, Tuscaloosa, Alabama 35487-0336, Biological Sciences Department, University of Alabama, Tuscaloosa, Alabama 35487, and Interdisciplinary Center for Information Technology, University of Alabama, Tuscaloosa, Alabama 35487-0336

Received: October 8, 2002; In Final Form: January 9, 2003

Carotenoids (Car), β-Carotene (I), 8′-apo-β-caroten-8′-al (II), and canthaxanthin (III), incorporated into activated Cu−MCM-41 were examined by UV/vis and EPR spectroscopies. A Cu^{2+}−Car complex was formed for I and III but not for II. Formation of a complex results in distortion of the all-trans carotenoid geometry and a tetragonal geometry for Cu^{2+}. The binding energies of Car and Cu^{2+}, the changes in the maximum absorption, and the bond lengths of Car after the formation of the Cu^{2+}−Car complex were examined by semiempirical ZINDO/1 and ZINDO/S calculations. Formation of a complex between Car and Cu^{2+} favors both forward and back electron transfer (ET) reactions due to the short distance (∼2 Å) between Car and Cu^{2+}, and reversible ET appears upon temperature cycling.

Introduction

Photoinduced electron transfer in heterogeneous hosts[1−3] has recently attracted more and more interest. Vesicles, micelles, molecular sieves, layered oxide materials, and silica gel have been found to be good photoredox systems for solar energy conversion and storage.[4−8] The photoinduced electron transfer in these hosts with various dyes has been studied. It is known that carotenoids (Car) serve as light harvesting and photoprotection agents in photosynthetic centers,[9,10] where they are also involved in the electron transfer (ET) chain resulting in $Car^{\bullet+}$ formation.[11] To understand the photophysical properties of Car, ET reactions of Car need to be studied. The diffusion controlled bimolecular ET reactions between Car and an electron acceptor in solution are not applicable because of the short lifetime of carotenoid excited states.[12] However, carotenoids locked in an appropriate orientation relative to acceptor molecules are photochemically reactive.[13,14] ET reactions of Car in liposomes,[15] TX100 micelles,[16] and sol−gels,[17] have been studied in our laboratory.

MCM-41 is a new family of mesoporous molecular sieves with uniform hexagonal pores varying from 15 Å to greater than 100 Å in size depending on the chain length of the micellar surfactant template used in the synthesis.[18−20] The surface area is about 1000 m^2/g and the pore size distribution is similar to that of zeolites. Previous studies[21,22] have shown that such materials can achieve long-lived photoproduced charge separation. In this research, a C_{16} chain length of micellar surfactant was employed as a template leading to an internal diameter of the mesoporous material of about 38 Å.[23] Because the length of most carotenoids is less than 30 Å (for example, the length of β-carotene is about 25 Å[24]), the carotenoids can be incorporated into the MCM-41 pores.

We are particularly interested in MCM-41 substituted with different transition-metal ions. Transition-metal complexes with organic ligands are of paramount interest.[25] The bonding in a transition-metal−olefin complex is often described by the Dewar−Chatt−Duncanson model:[26,27] electron donation from a filled π-orbital of an olefin into vacant s-, p-, or d-orbitals of the metal and binding overlap between an occupied d-orbital of metal with the empty π*-orbital of the olefin (π-back-donation). Although transition-metal complexes with unsaturated ligands such as ethylene have been extensively studied,[25,28,29] no report was found about interactions between transition-metal ions and long unsaturated ligands such as carotenoids. In the present study, we examined the electron transfer and interaction between carotenoids and Cu^{2+}. We chose Cu^{2+}-substituted MCM-41 (Cu−MCM-41) because copper complexes are well suited for EPR investigations, because the d^9 Cu^{2+} ion is subject to Jahn−Teller distortion so that axial and equatorial coordination sites become easily distinguishable.[30] For an elongated octahedral or square pyramidal coordination geometry with a $d_{x^2-y^2}$ ground state, the EPR spectrum shows $g_\perp < g_\parallel$;[31] for a trigonal bipyramidal coordination geometry with a d_{z^2} ground state, the spectrum shows $g_\perp > g_\parallel$.[32,33] β-Carotene (I), 8′-apo-β-caroten-8′-al (II), and canthaxanthin (III) (see Chart 1) were used in the present study. These three carotenoids with different terminal electron-withdrawing groups were incorporated in Cu−MCM-41 and their ET properties were investigated by EPR and UV/vis spectroscopies. Semiempirical ZINDO/1 and ZINDO/S calculations were performed to determine the binding energy and distance between Car and Cu^{2+} ions. Possible reaction products were identified by HPLC.

Experimental Section

Synthesis of MCM-41 and Cu−MCM-41. The procedure used for the preparation of the siliceous material (MCM-41) was similar to that reported by Beck et al.[18] First, tetrabutylammonium silicate (TBAS) was prepared in a 10:1 ratio (w/w) from tetrabutylammonium hydroxide (40 wt %, Aldrich) and

* To whom correspondence should be addressed. E-mail: lkispert@bama.ua.edu. Fax: (205) 348 9104.
[†] Department of Chemistry.
[‡] Biological Sciences Department.
[§] Interdisciplinary Center for Information Technology.

10.1021/jp027164h CCC: $25.00
Published on Web 02/22/2003

CHART 1: Structures of I−III

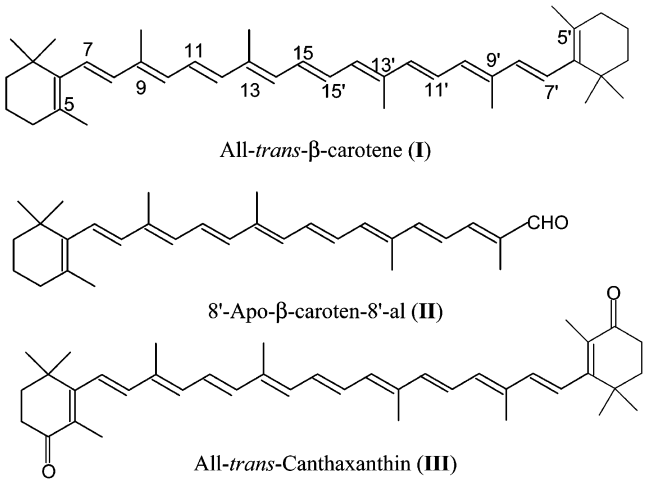

fumed silica (Sigma). Then 20.3 g of cetyltrimethylammonium chloride (CTAC, 25 wt %, Aldrich) and 12.21 g of TBAS were mixed with 5.94 g of H_2O. Finally, 5.91 g of fumed silica was dissolved in the mixture. The resulting gel was placed in a Teflon bottle and heated for 6 days at 95 °C, cooled to room temperature, washed with deionized water, and finally dried in air. The template CTAC was removed by calcination in air at 530 °C for 18 h. The resulting white powder is called MCM-41.

Cu−MCM-41 was prepared by liquid-state ion exchange according to the method of Xu et al.[34] Fifty milliliters of aqueous 1, 2, 4, and 6 mM Cu $(CH_3COO)_2 \cdot H_2O$ (98 wt %, Fisher) solution was added to four 0.5 g samples of MCM-41. The resulting mixtures were stirred for 24 h at room temperature, and then the samples were filtered and washed with hot deionized water (70 °C) to remove any ions adsorbed on the external surface. These are designated fresh Cu−MCM-41 with four different concentrations of Cu^{2+} in the four samples. The Cu/Si atomic ratios of the four Cu−MCM-41 samples were measured by a scanning electron microscope with an energy-dispersive X-ray analysis unit. The ratios are 0.014, 0.02, 0.038, and 0.046.

Chemicals. 8′-Apo-β-caroten-8′-al and canthaxanthin were purchased from Fluka (Buchs, Switzerland), β-carotene was from Sigma, and anhydrous dichloromethane was from Aldrich.

Sample Preparation. Fresh Cu−MCM-41 was dried at 110 °C for 3 h. A 100 mg amount of the dried sample was activated at 200 °C for 6 h, then at once transferred to a N_2 drybox, and allowed to cool to room temperature. Four milliliters of carotenoid CH_2Cl_2 solution of the desired concentration was prepared and added in the drybox, carotenoid was allowed to diffuse into the Cu−MCM-41 for 10 min, the mixture was stirred to evaporate the solvent, and the residue was transferred to an EPR tube, which was then stoppered. The EPR tube was taken out of the drybox, and residual solvent was removed under vacuum.

Instrumentation. X-ray powder diffraction (XRD) data were obtained from thin layers of samples, and measurements were carried out with a Philips 1840 diffractometer using Cu Kα radiation ($\lambda = 1.541$ Å) within the scattering angle 2θ range of 1.5−10°.

A S-2500 HITACHI scanning electron microscope with a TRACOR NORTHERN energy-dispersive X-ray analysis unit was used to measure the concentration of Cu^{2+} in Cu−MCM-41. The X-ray energy used in the measurements was 25 KV.

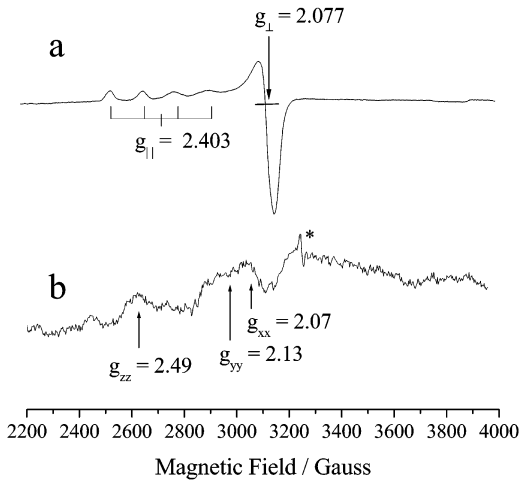

Figure 1. (a) EPR spectrum of fresh Cu−MCM-41, measured at 77 K. (b) EPR spectrum of Cu−MCM-41 after it was dehydrated at 110 °C K for 3 h, activated at 200 °C for 6 h, evacuated at room temperature, and then measured at 77 K. (* identifies the signal from the dewar).

EPR measurements were carried out with an X-band (9.5 GHz) Varian (Palo Alto, CA) E-12 EPR spectrometer, equipped with a rectangular cavity. The magnetic field was measured with a Bruker (Billerica, MA) EPR 035M gaussmeter, and the microwave frequency was measured with a model HP 5245L frequency counter.

A 250 W xenon lamp (ILC Technology) at a distance of 20 cm was used to irradiate the samples. Deionized water contained in a cylindrical glass cell (path length, 10 cm) was used as an IR cutoff filter. An optical filter was used to cut off most of the UV light below 350 nm.

A Vydac 201 TP54 polymeric C_{18} column (250 × 4.6 mm i.d.) packed with 5 μm particles (Hesperia, CA) and a Shimadzu LC-600 pump with a SPD-M10AVP PDA detector were used for the HPLC separation and detection. Acetonitrile was used as the mobile phase.

Optical spectra were recorded with a double beam Shimadzu UV−visible 1601 spectrophotometer (190−1100 nm). MCM-41 and Ti−MCM-41 samples were made into thin films by pressing the samples between two quartz plates; then the plates were sealed with scotch tape.

ZINDO/1[35] and ZINDO/S[36] calculations were performed using Hyperchem 6.03 software on a Dell computer (Pentium III).

Results and Discussion

The XRD patterns of siliceous MCM-41 measured after calcination are in accord with previously published results.[37] The data confirm the existence of the hexagonal MCM-41 lattice.[38] The Cu−MCM-41 showed the same XRD patterns, indicating that the ion-exchange does not damage the structure of MCM-41.

Figure 1a shows the EPR spectrum of fresh Cu−MCM-41 (Cu/Si = 0.038) with $g_{||} = 2.403$ and $g_\perp = 2.077$. These g values are close to $g_{||} = 2.400$ and $g_\perp = 2.079$ reported in the literature,[39] for the complex of Cu^{2+} after water was adsorbed on the activated Cu−MCM-41 (liquid-state ion-exchange). Three-pulse ESEEM spectra showed that this species is Cu^{2+} coordinated to six water molecules and that Cu^{2+} does not coordinate to the framework.[39] Figure 1b shows the EPR spectrum of Cu−MCM-41 (Cu/Si = 0.038) after Cu−MCM-41 was dehydrated at 110 K for 3 h, activated at 200 K for 6 h, evacuated at room temperature, and then measured at 77 K.

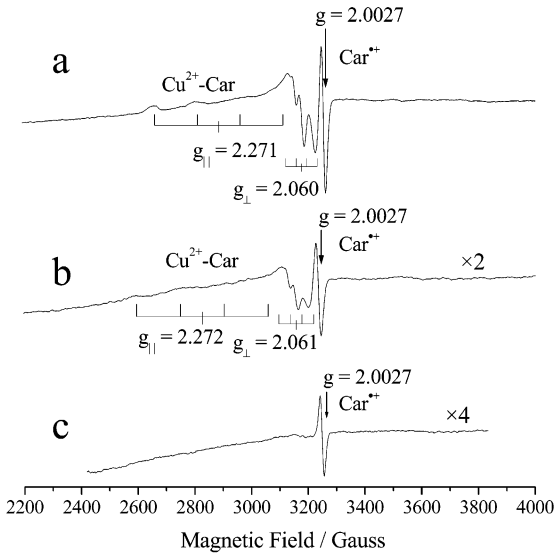

Figure 2. EPR spectrum of (a) I, (b) II, and (c) III adsorbed on activated Cu−MCM-41, measured at 77 K.

After dehydration, the EPR signal is very weak but is identical to that previously reported and analyzed by Kevan and coworkers.[39] The spectrum has been shown to be due to orthorhombic Cu^{2+} with g value equal to 2.07, 2.13, and 2.49, as obtained in Figure 1b. Whether the decrease in the Cu^{2+} signal intensity is caused only by the increase in the line width or by partial reduction of the Cu^{2+} ions is unclear.[39] The half field signal due to $Cu^{2+}-Cu^{2+}$ pairs[39] was not observed, probably due to the low concentration of Cu^{2+} in these samples.

Figure 2a shows the EPR spectrum after 20 μm of I was adsorbed on 100 mg of activated Cu−MCM-41 (Cu/Si = 0.038), measured at 77 K. Two sets of signals appear. One is due to Cu^{2+} with hyperfine splitting in the $g_\perp$ region. The other with peak to peak line width ΔH_{pp} of about 14 G and $g = 2.0027$ is the typical carotenoid radical cation ($Car^{\bullet+}$) signal.[40,41] The two signals overlap somewhat. We suggest that the formation of $Car^{\bullet+}$ is due to the oxidation of Car by Cu^{2+} when the solution of I diffused into Cu−MCM-41:

$$Car + Cu^{2+} \rightleftharpoons Car^{\bullet+} + Cu^{+}$$

The measured g values for Cu^{2+} (Figure 2a) are $g_{||} = 2.271$ and $g_\perp = 2.060$. The hyperfine constants are $A_{||} = 0.0172$ cm^{-1} and $A_\perp = 0.0026$ cm^{-1}. This Cu^{2+} signal shows that $g_{||} \gg g_\perp > 2.0023$ and $A_{||} \gg A_\perp$ typical for a tetragonally square pyramidal coordination geometry of a Cu^{2+} complex corresponding to a $d_{x^2-y^2}$ ground state of copper unpaired electron.[31,42] It was reported[39] that Cu^{2+} ion four-coordinates to the framework oxygen atoms in Cu−MCM-41 after dehydration of Cu−MCM-41. Previous studies[43−46] showed that when ethylene is adsorbed on a matrix containing Cu^{2+}, one Cu^{2+} interacts with only one ethylene molecule. Because Car is much larger than ethylene, one Cu^{2+} should interact with only one Car in Cu−MCM-41. When I interacts with Cu^{2+}, it replaces one silanol ligand forming a tetragonally square pyramidal coordination. The proposed tetragonal geometry is shown in Chart 2. This structure is supported by the fact[39,43−46] that interaction between Cu^{2+} and other adsorbed molecules causes rupture of some of Cu−O bonds. The number of Cu−O bonds broken depends on the bonding between Cu^{2+} and the framework and the binding between Cu^{2+} and the adsorbed molecules.[39,45] It has been reported that bonding of Cu^{2+} to the MCM-41 framework is

CHART 2: Tetragonal Geometry of Cu^{2+}

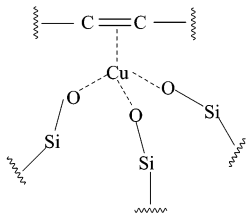

weak,[39] because adsorption of polar molecules such as H_2O and NH_3 removes Cu^{2+} from the four-coordinated sites, and Cu^{2+} coordinates to H_2O or NH_3.[39]

Figure 2b shows the EPR spectrum after 20 μm of II was imbedded in 100 mg of activated Cu−MCM-41 (Cu/Si = 0.038), measured at 77 K. The EPR spectrum is the same as that in Figure 2a except that the signals of the two species are weaker. Figure 2c shows the EPR spectrum after 20 μm of III was imbedded in 100 mg of activated Cu−MCM-41 (Cu/Si = 0.038), measured at 77 K. Only a weak signal with $g = 2.0027$ due to $Car^{\bullet+}$ of III appears. Because the $Car^{\bullet+}$ signal is weak, the possibility that all Cu^{2+} ions are reduced by III is ruled out. The absence of the $Cu^{2+}-Car$ signal indicates that III does not interact with Cu^{2+}. This is attributed to the special orientation of III in MCM-41.[37] The oxygen atoms in the cyclohexene ring of III may H-bond to −SiOH groups on the surface of the solid hosts and the ring methyl groups cause the chain to be located away from the surface of the pore. II may also H-bond to the −SiOH groups on the surface of the solid hosts, but the chain can still have access to the surface. The intensity of $Cu^{2+}-$Car(II) is lower than that of $Cu^{2+}-$Car(I), indicating that complex formation of Cu^{2+} and II is relatively difficult compared with that of Cu^{2+} and I. The decrease in the intensity of $Car^{\bullet+}$ from I to II to III after they diffuse into Cu−MCM-41 parallels the first oxidation potentials (vs SCE) of I−III in CH_2Cl_2 (0.63,[47] 0.72,[48] and 0.77 V,[47] respectively).

Figure 3a shows the dependence of the EPR signal intensities on the carotenoid concentration in CH_2Cl_2 solutions. The maximum $Car^{\bullet+}$ intensity occurs when the Cu−MCM-41 pores are saturated by carotenoid at about 20 μm/mg (5 mM of solution). Figure 3b shows the dependence of the EPR intensity of $Car^{\bullet+}$ on the concentration of Cu^{2+} ions in Cu−MCM-41. The signal intensity is saturated at Cu/Si = 0.038, so that Cu/Si = 0.038 is suitable for studying electron transfer reactions in Cu−MCM-41. (All samples were measured under the same EPR settings, and each point is an average of three experiments).

Optical studies were also carried out to understand the interaction between Car and Cu^{2+}. UV/vis absorption spectra for I and III imbedded in MCM-41 and Cu−MCM-41 are shown in Figure 4a,b, respectively. Because the samples were thin films, which diffract light, the spectral lines are irregular. The three vibronic bands characteristic of long chain polyenes are not resolved due to broadening of these bands in a polar environment.[49] The maximum absorption wavelengths (λ_{max}) of I and III in MCM-41 are 490 and 570 nm, respectively, and show a large red shift compared with that observed in CH_2Cl_2 (λ_{max} of I and III in CH_2Cl_2 are 460 and 555 nm, respectively). This phenomenon agrees with the large red-shifted absorbance of Car in the polar proteinous environment of RCs that has been attributed to mutual polarizability interactions between Car and the surrounding medium.[50] On the other hand, the λ_{max} of I in Cu−MCM-41 is large blue shifted (about 70 nm) compared to that in MCM-41, indicating that I interacts with Cu^{2+}. According to previous studies,[37] the blue shift is due to the decrease in π-conjugation of Car because of conformational changes of Car

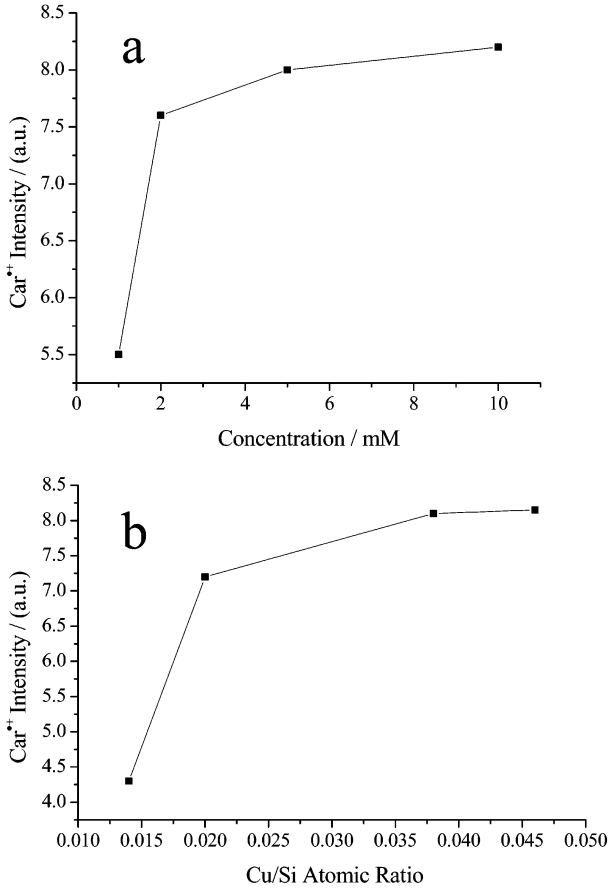

Figure 3. (a) EPR signal intensities of I cation radicals when 100 mg of Cu−MCM-41 and 4 mL of 1, 2, 5, and 10 mM I−CH_2Cl_2 solution were used to prepare the sample. (b) EPR signal intensities of I cation radicals after 4 mL of 5 mM I CH_2Cl_2 solution and 100 mg of Cu−MCM-41 with four different concentrations of Cu were used to prepare the sample. The Cu/Si atomic ratios of Cu−MCM-41 are 0.014, 0.02, 0.038, and 0.046.

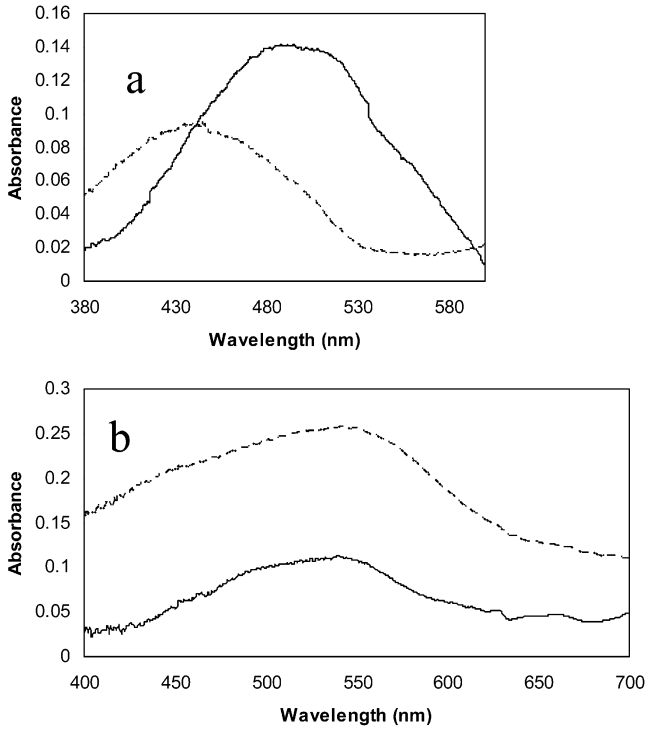

Figure 4. UV/vis spectra of (a) I and (b) III imbedded in MCM-41 and Cu−MCM-41. The solid line is that for Car imbedded in MCM-41, and the dashed line is that for Car imbedded in Cu−MCM-41.

when it interacts with transition metal ions. No significant change was found for III (the difference in λ_{max} is within the measurement error range), indicating that III does not interact with Cu^{2+}.

ZINDO/1[35] and ZINDO/S[36] semiempirical calculations were carried out to understand the conformational change of Car and the blue shift in the optical spectra. The ZINDO/1[35] method is widely used for the determination of structures and energies of complexes with first and second row transition metals. On the other hand, the ZINDO/S[36] method is more useful for predicting UV/vis spectra. A series of Cu^{2+}−Car complex conformations was obtained depending on the initial position of Cu^{2+} around the conjugated chain of Car during the geometry optimization. The optimized geometries of I and three Cu^{2+}−I complexes by ZINDO/1 are shown in Figure 5. The initial positions of Cu^{2+} for the geometries of the complexes in Figure 5b,c,d were to center Cu^{2+} at ∼3 Å opposite C13═C14, C7═C8 and C15═C15′ double bonds, respectively. Unrestricted Hartree−Fock (UHF) formalism was used for the optimization. After optimizing the structure, the chain of I is significantly distorted. The binding energies (BE) of Cu^{2+} and I and bond lengths calculated by ZINDO/1 are also shown in Figure 5. The calculation shows that the BEs depends on the location of Cu^{2+} along the chain of Car, for example, the BEs for the complex in Figure 5b,c,d are 63.9, 147.9, and 232.8 kcal/mol, respectively. The bond lengths also change: the double bond lengths increase and the single bond lengths decrease. These changes are more significant in the vicinity of Cu^{2+}. For example, the C13═C14 double bond and C8−C9 single bond in Figure 5b change from 1.448 to 1.416 Å and from 1.366 to 1.470 Å, respectively; the C7═C8 double bond and C6−C7 single bond in Figure 5c change from 1.353 to 1.467 Å and from 1.454 to 1.416 Å, respectively; and the C15═C15′ double bond and C14−C15 single bond in Figure 5d change from 1.358 to 1.455 Å and from 1.437 to 1.374 Å, respectively. It has been suggested[51] that distortion of the π conjugated system causes the rehybridization of carbon and thus causes the bond length change. The reason for the rehybridization is that the distortion causes loss of overlap of the two p orbitals. To regain some of the p orbital overlap, the doubly bonded carbons undergo a rehybridization.[52] The calculated distance between Cu^{2+} and the nearest bond of I is in the range of 1.9−2.0 Å. The spectral maxima of I and the complexes by ZINDO/S calculation are also shown in Figure 5. The single-excitation configuration interaction involving about 100 configurations was used to calculate the optical absorption spectrum. The calculated spectral maxima of I is 432 nm and those of complexes are 355 (Figure 5b), 348 (Figure 5c), and 285 nm (Figure 5d), which shows that λ_{max} of the complex is blue shifted compared to that of I.

Electron transfer of I imbedded in Cu−MCM-41 was studied by EPR spectroscopy. Figure 6a shows the EPR spectra of the sample shortly after preparation (solid line) and storing at room temperature for 2 (dashed line) and 4 h (dotted line). During the sample preparation, $Car^{\bullet+}$(I) was produced by oxidation of I with Cu^{2+} when I (in CH_2Cl_2) was diffused into the pores of Cu−MCM-41. After CH_2Cl_2 was removed, back electron transfer from Cu^+ to $Car^{\bullet+}$ was indicated by a decrease of the $Car^{\bullet+}$ signal and an increase of the Cu^{2+}−Car signal. After 4 h, the ET reaction was complete. The narrow peak with g value 2.0023 is due to the dewar. Figure 6b shows the EPR spectrum of the dewar. The back ET reaction is probably due to the relative ground-state energy change of $Car^{\bullet+}$ and Cu^+ after solvent CH_2Cl_2 removal. The ground-state energy of $Car^{\bullet+}$ is

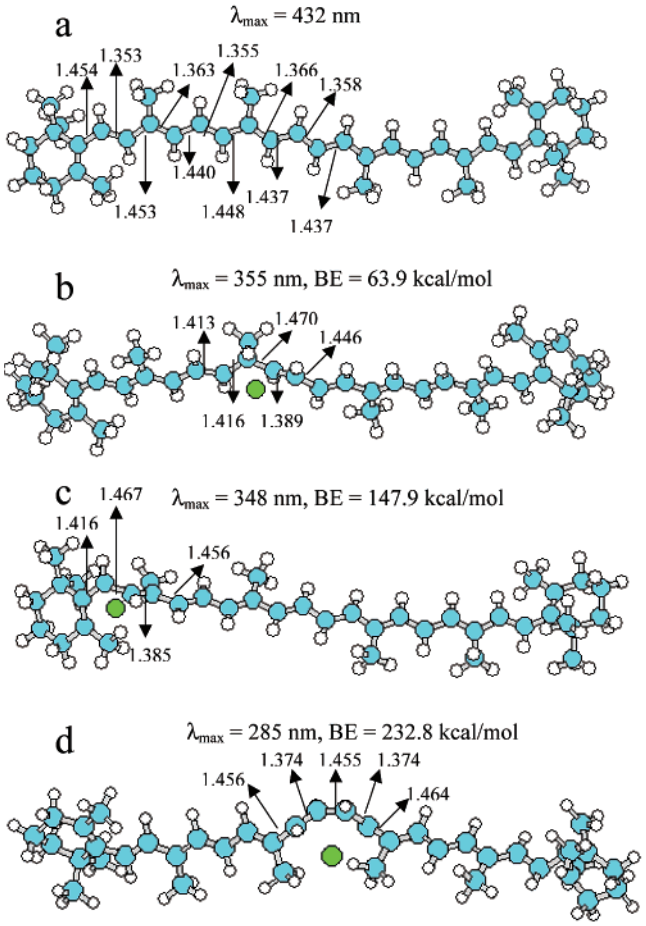

Figure 5. Geometries of (a) I and (b)−(d) complexes of I and Cu^{2+} by ZINDO/1 geometry optimizations. (b)−(d) Complexes obtained with the initial position of Cu^{2+} located near C13═C14, C7═C8, and C15═C15′ bonds, respectively. The binding energy and bond length are calculated by ZINDO/1. The λ_{max} of the strongest peak is calculated by ZINDO/S.

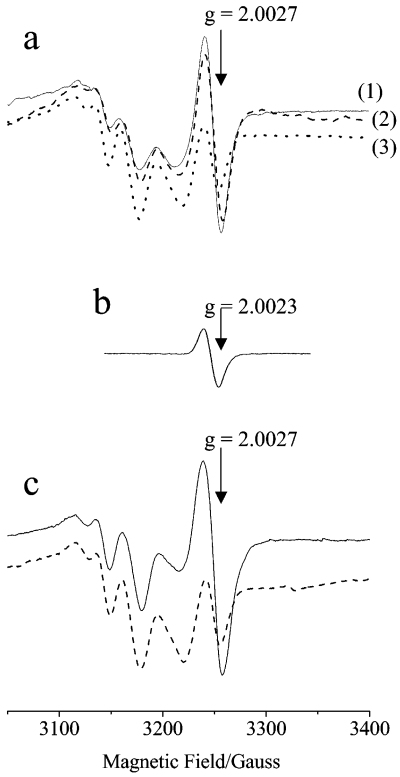

Figure 6. (a) Solid line (1), EPR spectrum of I embedded in activated Cu−MCM-41; dashed line (2), 2 h later at room temperature; dotted line (3), 4 h later at room temperature. (b) EPR spectrum of the dewar. (c) Solid line, EPR spectrum after re-photoirradiation of the above EPR sample at 77 K; dashed line, 1 min later at room temperature. All EPR measurements were performed at 77 K.

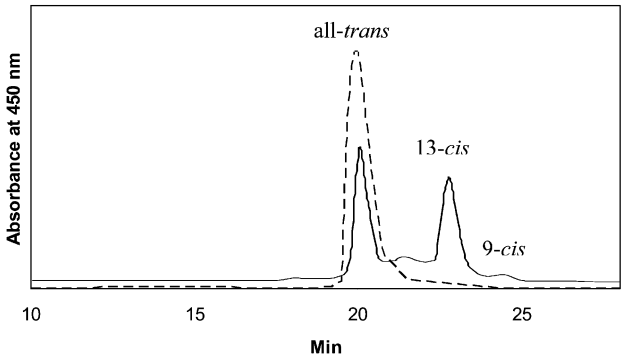

Figure 7. Solid line: HPLC of the extraction from the EPR sample after back electron transfer at room temperature. Dashed line: HPLC of I.

lower than that of Cu^{+} in Cu−MCM-41 at room temperature and causes the ET from Cu^{+} to $Car^{\bullet+}$. After photoirradiation of the sample at 77 K, electron transfer from I to Cu^{2+} was observed by the decrease of the Cu^{2+}−Car signal and an increase of the $Car^{\bullet+}$ signal (solid line in Figure 6c). After warming the sample to room temperature for 1 min, back ET from Cu^{+} to $Car^{\bullet+}$ was complete (dashed line in Figure 6c). Back ET in a re-irradiated sample is faster than in the initial sample. To understand this phenomenon, we examined the reaction products after the initial back ET reaction by HPLC. HPLC analysis of the reaction products (CH_2Cl_2 was used to extract products) is shown in Figure 7. After the initial back ET reaction, two *cis*-isomers of I were detected. No other decay products were found. Identification of the *cis*-isomers is based on our previous results.[53−55] ^{1}H NMR spectroscopy and values of the *Q* ratio[56] (absorbance of the "cis peak"/absorbance of the most intense maximum) were used to identify these isomers. The proposed isomerization mechanism is

$$\textit{trans}\text{-Car}^{\bullet+} \rightleftharpoons \textit{cis}\text{-Car}^{\bullet+}$$

$$\textit{cis}\text{-Car}^{\bullet+} + Cu^{+} \rightleftharpoons \textit{cis}\text{-Car} + Cu^{2+}$$

This mechanism is supported by the previous result[53−55] that isomerization is facile via $Car^{\bullet+}$. Both *trans*-$Car^{\bullet+}$ and *cis*-$Car^{\bullet+}$ are involved in the two back ET reactions, and the electron acceptors in the two cases are the same. The different ET transfer rates in the two cases can be attributed to the difference in the distances between the donor Cu^{+} and the acceptors $Car^{\bullet+}$ in the two cases. According to Figure 6a, formation of the Cu^{2+}−Car complex occurs during the back ET reaction. The reaction mechanism is

$$Car^{\bullet+} + Cu^{+} \rightarrow Car + Cu^{2+} \rightarrow Cu^{2+}\text{−Car}$$

This indicates that there is movement of Car in Cu−MCM-41 during or after the back ET reaction. After photoirradiation, the complex Cu^{+}−$Car^{\bullet+}$ forms. In the Cu^{+}−$Car^{\bullet+}$ complex, back ET from Cu^{+} to $Car^{\bullet+}$ can be treated as intramolecular because the orbitals of donor and acceptor overlap. So the ET is fast. The reason the initial back ET reaction is very slow is probably because Cu^{+} and $Car^{\bullet+}$ do not form complexes after the chemical oxidation of Car with Cu^{2+} when Car is diffused into

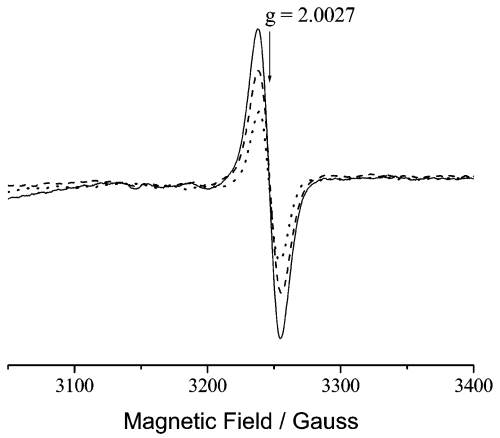

Figure 8. Solid line: EPR spectrum after photoirradiation of III imbedded in Cu−MCM-41. Dashed line: 10 min later at room temperature. Dotted line: 20 min later at room temperature.

Cu−MCM-41. The electron transfer is intermolecular and thus is slow because of the approximately exponential decrease of ET rates with increasing distance.[57] For a nonadiabatic ET reaction, the rate constant is generally described as[58]

$$k_{ET} = (4\pi^2/h)|V|^2 FC$$

where V is the electronic coupling matrix element and FC is the Franck−Condon weighted density of the states. Because V depends on the overlap of the molecular orbitals associated with the donor and acceptor moieties, it is sensitive to distance and is commonly modeled by[58]

$$|V|^2 = |V_0|^2 \exp(-\beta r_{DA})$$

whereV_0 and β are constants and r_{DA} is the distance between the donor and acceptor. β is on the order of 2.8 $Å^{-1}$ for "through-space" electron transfer.

To confirm that the back ET rate constant is distance-dependent, III imbedded in Cu−MCM-41 was photoirradiated to produce $III^{\bullet+}$ and the back ET reaction from Cu^+ to $III^{\bullet+}$ at room temperature was studied by EPR spectroscopy (Figure 8). Because III does not form a complex with Cu^{2+}, the back ET from Cu^+ to $III^{\bullet+}$ is slower than that of $Cu^+-I^{\bullet+}$ although $III^{\bullet+}$ contains two strong electron-withdrawing groups. After reacting for 20 min at room temperature, a significant amount of $III^{\bullet+}$ was present in the sample.

How the formation of complexes affects the forward ET from Car to Cu^{2+} is also important. The photoyields of $Car^{\bullet+}$(I−III) imbedded in Cu−MCM-41 were compared to those in MCM-41. The $Car^{\bullet+}$ photoyields in Cu−MCM-41 were measured for samples with Cu^{2+}−Car complex formation. These samples were photoirradiated at 77 K for 5 min, and then EPR measurements were performed at 77 K. The photoyields of $I^{\bullet+}$, $II^{\bullet+}$ and $III^{\bullet+}$ are shown in Figure 9. In MCM-41; the photoyield decreases in the order I > II > III. This agrees with the previous result that the photoyield of Car in MCM-41 is high for Car with low oxidation potential.[37] The introduction of Cu^{2+} into MCM-41 causes enhancement in photoyield for all carotenoids studied here. The enhancement decreases significantly in the order I > II > III because I easily forms complexes with Cu^{2+} and thus electron transfer from I to Cu^{2+} is favored; III does not form complexes with Cu^{2+} and the photoyield enhancement is very low. II partially forms complexes with Cu^{2+} so the photoyield enhancement is lower than that of I and higher than that of III. This result is consistent with the previous study[37] that the photoyield of Car in Ti−MCM-41 depends on the complex formation of Car and Ti^{4+}.

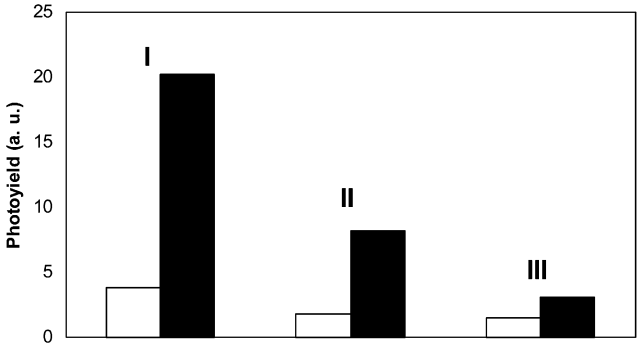

Figure 9. Photoyield comparison of I−III imbedded in MCM-41 and Cu−MCM-41. Blank columns represent the photoyield in MCM-41; black columns represent that in Cu−MCM-41. The error in the photoyield measurements is estimated to be ±10%.

Conclusions

Interaction between carotenoids and Cu^{2+} in Cu−MCM-41 causes conformational changes of the carotenoid and causes a large blue shift in the maximum absorption of carotenoid due to a decrease in the π conjugation. The interaction also causes an increase in the double bond lengths and a decrease in the single bond lengths for Car. These changes are more significant in the vicinity of Cu^{2+}. The binding energy of Cu^{2+} to carotenoid depends on the location of Cu^{2+} along the chain of Car. The highest BE is about 232 kcal/mol when Cu^{2+} forms a complex at C15═C15′ double bond. The distance between Cu^{2+} and carotenoid in the Cu^{2+}−Car complex is short (∼2 Å) and favors light-driven electron transfer from Car to Cu^{2+} and also permits the thermal back electron transfer rate from Cu^+ to $Car^{\bullet+}$. This study shows that the interaction between Car and electron acceptor can increase the photoyield of $Car^{\bullet+}$ and is largest for β-carotene and Cu^{2+}. The saturated concentration of Car in MCM-41 of about 20 μm/100 mg and the ratio of Cu/Si of about 0.04 is suitable for studying ET reactions of dye in Cu−MCM-41.

Acknowledgment. Dr. Langqiu Xu (Argonne National Laboratory) and the late Dr. Larry Kevan (Chemistry Department, University of Houston) are thanked for providing suggestions for synthesizing MCM-41 and Cu-MCM-41. Dr. Elli Hand is thanked for helpful discussions. This work was supported by the Chemical Sciences, Geosciences and Biosciences Division, Office of Basic Energy Sciences, Office of Science, U.S. Department of Energy, under Grant No. DE-FG02-86ER 13465.

References and Notes

(1) Kalyanasundaram, K. *Photochemistry in Microheterogeneous Systems*; Academic Press: New York, 1987.

(2) (a) *Energy Resources through Photochemistry and Catalysis*; Grätzel, M., Ed.; Academic Press: New York, 1983. (b) Grätzel, M. *Heterogeneous Photochemical Electron Transfer*; CRC Press: Boca Raton, FL, 1988.

(3) *Photochemical Conversion and Storage of Solar Energy*; Connolly, J. S., Ed.; Academic Press: New York, 1981.

(4) Kevan, L. In *Photoinduced Electron-Transfer Part B*; Fox, M. A., Chanon, M., Eds.; Elsevier: Amsterdam, 1988; p 329.

(5) Hurst, J. K.; Lee, L. Y. C.; Graetzel, M. J. *J. Am. Chem. Soc.* **1983**, *105*, 7048.

(6) (a) Corma, A.; Fornes, V.; Garcia, H.; Miranda, M. A.; Sabater, M. J. *J. Am. Chem. Soc.* **1994**, *116*, 9767. (b) Gener, I.; Buntinx, G.; Bremard, C. *Angew. Chem., Int. Ed. Engl.* **1999**, *38*, 1819. (c) Borja, M.;

Dutta, P. K. *Nature* **1993**, *362*, 43. (d) Ledney, M.; Dutta, P. K. *J. Am. Chem. Soc.* **1995**, *117*, 7687.

(7) (a) Krishna, R. M.; Kurshev, V.; Kevan, L. *Phys. Chem. Chem. Phys.* **1999**, *1*, 2833. (b) Krishna, R. M.; Kevan, L. *Micropor. Mesopor. Mater.* **1999**, *32*, 169.

(8) (a) Xiang, B.; Kevan, L. *Langmuir* **1994**, *10*, 2688. (b) Xiang, B.; Kevan, L. *J. Phys. Chem.* **1994**, *98*, 5120.

(9) Koyama, Y. *J. Photochem. Photobiol. B* **1991**, *9*, 265.

(10) Koyama, Y.; Kuki, M.; Andersson, P. O.; Gillbro, T. *Photochem. Photobiol.* **1996**, *63*, 243.

(11) Faller, P.; Pascal, A.; Rutherford, A. W. *Biochemistry* **2001**, *40*, 6431.

(12) Pan, J.; Benkö, G.; Xu, Y.; Pascher, T.; Sun, L.; Sundström, V.; Polívka, T. *J. Am. Chem. Soc.* **2002**, *124*, 13949.

(13) Sereno, L.; Silber, J. J.; Otero, L.; del, Valle Bohorquez, M.; Moore, A. L.; Moore, T. A.; Gust, D. *J. Phys. Chem.* **1996**, *100*, 814.

(14) Gao, F. G.; Bard, A. J.; Kispert, L. D. J. *Photochem. Photobiol. A* **2000**, *130*, 49.

(15) He, Z.; Kispert, L. D.; Metzger, R. M.; Gosztola, D.; Wasielewski, M. R. *J. Phys. Chem. B* **2000**, *104*, 6302.

(16) He, Z.; Kispert, L. D. *J. Phys. Chem.* **1999**, *103*, 9038.

(17) He, Z. Dissertation of The University of Alabama.

(18) Beck, J. S.; Vartuli, J. C.; Roth, W. J.; Leonowicz, M. E.; Kresge, C. T.; Schmitt, K. D.; Chu, T.-W.; Olson, D. H.; Sheppard, E. W.; McCullen, S. B.; Higgins, J. B.; Schlenker, J. L. *J. Am. Chem. Soc.* **1992**, *114*, 10834.

(19) Casci, J. L. In *Advanced Zeolite Science and Application Studies*; Jansen, J. C., Stöcker, M., Karge, H. G., Weitkamp, J., Eds.; Elsevier: Amsterdam, 1994; Vol. 85, p 329.

(20) Chen, C.-Y.; Li, H.-X.; Davis, M. E. *Micropor. Mater.* **1993**, *2*, 17.

(21) Sung-Suh, H. M.; Luan, Z.; Kevan, L. *J. Phys. Chem. B* **1997**, *101*, 10455.

(22) Krishna, R. M.; Prakash, A. M.; Kevan, L. *J. Phys. Chem. B* **2000**, *104*, 1796.

(23) Kruk, M.; Jaroniec, M.; Sakamoto, Y.; Terasaki, O.; Ryoo, R.; Ko, C. H. *J. Phys. Chem. B* **2000**, *104*, 292.

(24) Johansson, L. B. A.; Lindblom, G.; Wieslander, A.; Arvidson, G. *FEBS Lett.* **1981**, *128*, 97.

(25) (a) Freiser, B. S. *Chemtracts: Anal. Phys. Chem.* **1989**, *1*, 65. (b) Armentrout, P. B. *Annu. Rev. Phys. Chem.* **1990**, *41*, 313. (c) Eller, K.; Schwarz, H. *Chem. Rev.* **1991**, *91*, 1121. (d) Tsipis, C. A. *Coord. Chem. Rev.* **1991**, *108*, 163. (e) Veillard, A. *Chem. Rev.* **1991**, *91*, 743. (f) Weishaar, J. C. *Acc. Chem. Res.* **1993**, *26*, 213.

(26) Dewar, M. J. S. *Bull. Soc. Chim. Fr.* **1951**, *C79*, 18.

(27) Chatt, J.; Duncanson, L. A. *J. Chem. Soc.* **1953**, 2939.

(28) Sodupe, M.; Bauschlicher, C. W. *J. Phys. Chem.* **1991**, *95*, 8640.

(29) Sodupe, M.; Bauschlicher, C. W.; Langhoff, S. R.; Partridge, H. *J. Phys. Chem.* **1992**, *96*, 2118.

(30) Pilbrow, J. R. *EPR of Transition Metal Ions*; Clarendon Press: Oxford, U.K., 1990.

(31) Solomon, E. I.; Gewrith, A. A.; Westmoreland, T. D. *Advanced EPR, Application in Biology and Biochemistry*; Elsevier: Amsterdam, 1989; Chapter 25.

(32) Jiang, F.; Karlin, K. D.; Peisach, J. *Inorg. Chem.* **1993**, *32*, 2576.

(33) Karlin, K. D.; Tyeklar, Z. *Bioinorganic Chemistry of Copper*; Chapman and Hall: New York, 1993.

(34) Xu, J.; Yu, J.-S.; Lee, S. J.; Kim, B. Y.; Kevan, L. *J. Phys. Chem. B* **2000**, *104*, 1307.

(35) (a) Bacon, A. D.; Zerner, M. C. *Theor. Chim. Acta* **1979**, *53*, 21. (b) Zerner, M. C.; Loew, G. H.; Kirchner, R. F.; Mueller-Westerhoff, U. T. *J. Am. Chem. Soc.* **1980**, *102*, 589. (c) Anderson, W. P.; Edwards, W. D.; Zerner, M. C. *Inorg. Chem.* **1986**, *25*, 2728. (d) Culberson, J. C.; Knappe, P.; Rosch, N.; Zerner, M. C. *Theor. Chim. Acta* **1987**, *71*, 21. (e) Baker, J. D.; Zerner, M. C. *J. Phys. Chem.* **1990**, *94*, 2866. (f) Anderson, W.; Cundari, T.; Zerner, M. C. *Int. J. Quantum Chem.* **1990**, *39*, 31. (g) Anderson, W.; Cundari, T.; Drago, R.; Zerner, M. C. *Inorg. Chem.* **1991**, *29*, 1.

(36) (a) Ridley, J.; Zerner, M. C. *Theor. Chim. Acta* **1973**, *32*, 111. (b) Ridley, J.; Zerner, M. C. *Theor. Chim. Acta* **1976**, *42*, 223.

(37) Gao, Y.; Konovalova, T. A.; Xu, T.; Kispert, L. D. *J. Phys. Chem. B*, in press.

(38) (a) Kresge, C. T.; Leonowicz, M. E.; Roth, W. J.; Vartuli, J. C.; Beck, J. S. *Nature* **1992**, *359*, 710. (b) Beck, J. S.; Vartuli, J. C.; Roth, W. J.; Leonowicz, M. E.; Kresge, C. T.; Schmitt, K. D.; Chu, C. T.-W.; Olson, D. H.; Sheppard, E. W.; McCullen, B.; Higgins, J. B.; Schlenker, J. L. *J. Am. Chem. Soc.* **1992**, *114*, 10834. (c) Beck, J. S.; Vartuli, J. C.; Kennedy, G. J.; Kresge, C. T.; Roth, W. J.; Schramm, S. E. *Chem. Mater.* **1994**, *6*, 1816. (d) Vartuli, J. C.; Schmitt, K.; Kresge, C. T.; Roth, W. J.; Leonowicz, M. E.; McCullen, B.; Hellring, S. D.; Beck, J. S.; Schlenker, J. L.; Olson, D. H.; Sheppard, E. W. In *Zeolites and Related Microporous Materials: State of the Art 1994*; Weitkamp, J., Karge, H. G., Pfeifer, H., Holderich, W., Eds.; *Studies in Surface Science and Catalysis*; Elsevier: Amsterdam, 1994; Vol. 84, pp 53−60.

(39) Pöpple, A.; Newhouse, M.; Kevan, L. *J. Phys. Chem.* **1995**, *99*, 10019.

(40) Jeevarajan, A. S.; Khaled, M.; Kispert, L. D. *J. Phys. Chem.* **1994**, *98*, 7777.

(41) Jeevarajan, A. S.; Khaled, M.; Kispert, L. D. Chem. *Phys. Lett.* **1994,** *225*, 340.

(42) Kurdziel, K.; Głowiak, T.; Jezierska, J. *Polyhedron* **2001**, *20*, 3307.

(43) Kim, J. Y.; Yu, J.-S.; Kevan, L. *Mol. Phys.* **1998**, *95*, 989.

(44) Yu, J.-S.; Ryoo, W.; Kim, S. J.; Hong, S. B.; Kevan, L. *J. Phys. Chem.* **1996**, *100*, 12624.

(45) Ichikawa, T.; Yoshida, H.; Kevan, L. *J. Phys. Chem.* **1982**, *88*, 881.

(46) Narayana, M.; Zhan, R. Y.; Kevan, L. *J. Phys. Chem.* **1984**, *88*, 3990.

(47) Hapiot, P.; Kispert, L. D.; Konovalov, V. V.; Savéant, J.-M. *J. Am. Chem. Soc.* **2001**, *123*, 6669.

(48) Liu, D.; Gao, Y.; Kispert, L. D. *J. Electroanal. Chem.* **2000**, *488*, 140.

(49) O'Neil, M. P.; Wasielewski, M. R.; Khaled, M. M.; Kispert, L. D. *J. Chem. Phys.* **1991**, *95*, 7212.

(50) Andersson, P. O.; Gillbro, T.; Ferguson, L.; Cogdell, R. *J. Photochem. Photobio.* **1991**, *54*, 353.

(51) Yang, X.; Wang, G.; Yang, Z.; Shang, Z.; Cai, Z.; Pan, Y.; Wu, B.; Zhao, X. *Theochem* **2002**, *579*, 91. (b) Kovacek, D.; Margetic, D.; Maksic, Z. B. *Theochem* **1993**, *104*, 195. (c) Jursic, B. S. *Theochem* **1999**, *492*, 85. (d) Mittendorfer, F.; Hafner, J. *Surf. Sci.* **2001**, *472*, 133. (e) Eckert-Maksić, M.; Hodošček, M. Kovaček, D. Maksić, Z. B. Poljanec, K. *Chem. Phys. Lett.* **1990**, *171*, 49. (f) Chisholm, M. H.; Conroy, B. K.; Clark, D. L.; Huffman, J. C. *Polyhedron* **1988**, *7*, 903.

(52) (a) Marshall, J. A.; Faubl, H. *J. Am. Chem. Soc.* **1967**, *89*, 5965. (b) Köbrich, G. *Angew. Chem., Int. Ed. Engl.* **1973**, *12*, 464. (c) Buchanan, G. L. *Chem. Soc. Rev.* **1974**, *3*, 41.

(53) Gao, G.; Wei, C. C.; Jeevarajan, A. S.; Kispert, L. D. *J. Phys. Chem.* **1996**, *100*, 5362.

(54) Gao, G.; Deng, Y.; Kispert, L. D. *J. Phys. Chem. B* **1998**, *102*, 3897.

(55) Wei, C. C.; Gao, G.; Kispert, L. D. *J. Chem. Soc., Perkin Trans.* **1997**, *2*, 783.

(56) Dewar, M. J. S.; Zoebisch, E. G.; Healy, E. F.; Stewart, J. J. P. *J. Am. Chem. Soc.* **1985**, *107*, 3902.

(57) (a) Closs, G. L.; Miller, J. R. *Science* **1988**, *240*, 440. (b) Newton, M. D.; Sutin, N. *Annu. Rev. Phys. Chem.* **1984**, *35*, 437. (c) Guarr, T.; McLendon, G. *Coord. Chem. Rev.* **1985**, *68*, 1. (d) Hush, N. *S. Coord. Chem. Rev.* **1985**, *64*, 135. (e) Sutin, N. *Progr. Inorg. Chem.* **1983**, *30*, 441. (f) Marcus, R. A.; Sutin, N. *Biochim. Biophys. Acta* **1985**, *811*, 265.

(58) (a) Marcus, R. A.; Sutin, N. *Biochim. Biophys. Acta* **1986**, *811*, 265. (b) Kestner, N. R.; Jortner, J.; Logan, J. *J. Phys. Chem.* **1974**, *78*, 2148. (c) Brunschwig, B. S.; Logan, J.; Newton, M.; Sutin, N. *J. Am. Chem. Soc.* **1980**, *102*, 5798. (d) Gamow, G. *Z. Phys.* **1928**, *58*, 204. (e) Calude, J. P.; Meyer, T. J. *J. Phys. Chem.* **1995**, *99*, 51. (f) Chen, P.; Mecklenbur, S. L.; Meyer, T. J. *J. Phys. Chem.* **1993**, *97*, 13126.